processes

MDPI

Article

Bayesian-Optimized Machine Learning Framework with SHAP Interpretation for Rockburst Intensity Prediction in Deep Underground Engineering

Jinzhao Zhang [1], Libao Jia [1], Zhixin Ma [2] and Zongbin Wang [3,*]

[1] School of Modern Services, Harbin Vocational College of Science and Technology, Harbin 150300, China; zhangjz_hkzy@163.com (J.Z.); lipaochia@gmail.com (L.J.)
[2] China Construction Seventh Engineering Bureau Co., Ltd., Zhengzhou 450004, China; mzxcscec7b@163.com
[3] School of Civil and Hydraulic Engineering, Lanzhou University of Technology, Lanzhou 730050, China
* Correspondence: wangzongbin@lut.edu.cn; Tel.: +86-15332205334

Abstract

As mineral resource development moves deeper into the earth, mine dynamic disasters, represented by rockbursts, occur frequently. Due to the combined effects of in situ rock stress state and geostress conditions, it is difficult to obtain reliable prediction results using traditional empirical criteria or single-index prediction methods. To address these issues, this paper constructs a rockburst sample database based on the existing literature, including maximum tangential stress, uniaxial compressive strength, uniaxial tensile strength, elastic energy index, stress coefficient, and brittleness coefficient. Secondly, six typical machine learning algorithms are selected for rockburst level classification research. Then, to address the problem of imbalanced sample distribution, the SMOTE oversampling method is introduced to balance the data, and Bayesian optimization and cross-validation are combined to optimize the model hyperparameters. The results show that optimized XGBoost models exhibit high accuracy and stability in rockburst level discrimination, and accuracy reached 0.7664, recall was 0.7664, macro-P was 0.7664, and macro-F1 was 0.7662. Furthermore, taking the BO-XGBoost model as an example, the SHAP method is introduced to analyze the interpretability of the model's prediction results. The results show that the elastic energy index and stress-related indices are the main controlling factors affecting the intensity of rockburst; they accounted for 25.75% and 22.68%, respectively. Based on the above research results, this paper further explores the ideas for rockburst safety management and prevention from the aspects of energy control, stress regulation, and optimization of rock mass structural characteristics, providing theoretical basis and technical support for the scientific formulation of rockburst risk identification, level prediction, and safety prevention and control measures in deep underground engineering.

Keywords: rockburst prediction; machine learning; data oversampling; Bayesian optimization; model interpretability

Academic Editors: Tianshou Ma, Jiang Guo, Jiachuang Wang and Chengmin Wei

Received: 6 July 2026
Revised: 24 July 2026
Accepted: 27 July 2026
Published: 29 July 2026

1. Introduction

As the development of deep mineral resources gradually extends towards greater burial depths and higher stress levels, the phenomena of stress concentration and rapid accumulation of elastic energy within the surrounding rock are becoming increasingly significant, leading to frequent rock bursts and other rock dynamic disasters [1,2]. Rock bursts are typically sudden and have a concentrated destructive range, often exhibiting characteristics such as instantaneous fracturing and violent rock fragment ejection [3,4], posing a significant threat to life safety and equipment damage [5,6]. Therefore, conducting reasonable prediction and reliable evaluation of rock burst tendency is of great significance for the advanced identification of potential risk areas and mine production [4,7]. The incubation and occurrence of rock bursts are jointly controlled by multiple factors, including rock mechanical properties, the stress state of the original rock, rock mass structural characteristics, and energy accumulation and release processes, exhibiting significant nonlinear evolution and multi-source coupling characteristics. In complex deep engineering environments, traditional methods based on empirical criteria or single indicators are difficult to obtain accurate classification results [8,9]. Against this background, it is necessary to conduct systematic research on rock burst tendency prediction to provide a theoretical basis for the safety management and disaster prevention of deep underground engineering.

Early rockburst prediction mainly relied on empirical criteria and statistical analysis methods, usually selecting a single or a small number of parameters as the basis for judgment and then making a qualitative or semi-quantitative evaluation of the probability of rockburst occurrence. Such methods are relatively convenient to obtain parameters and have simple model structures, but single indicators are often difficult to fully characterize the rockburst occurrence mechanism under complex engineering conditions. Therefore, the prediction stability and generalization ability of such methods are limited to a certain extent [10]. With the development of multi-index comprehensive discrimination methods, some scholars have used mathematical models to analyze rockburst classification. For example, Owusu-Ansah et al. [11] used the decision tree model to classify rockbursts. Through comparison and analysis with various algorithms, it can be seen that the unified decision tree model has advantages such as simple structure and strong interpretability when dealing with rockburst classification problems. Sun et al. [12] proposed a rockburst prediction method based on RF-CRITIC and improved cloud model. By optimizing the weight of evaluation indicators and introducing microseismic parameters, the prediction accuracy and applicability of the model were effectively improved. Hafiz et al. [13] conducted research on rockburst prediction based on the KNN algorithm and pointed out that the fit between the algorithm characteristics and the rockburst mechanical mechanism is more important in improving the accuracy of rockburst classification. Hu et al. [14] improved the normal cloud model in response to the fuzzy uncertainty in the rockburst prediction process and improved the reliability of rockburst tendency evaluation by integrating multiple weighting methods through game theory. Chuai et al. [15] constructed a multi-index rockburst prediction model based on the analytic hierarchy process and fuzzy mathematics theory, comprehensively introducing key factors about stress state and surrounding rock structure. Xue et al. [16] significantly reduced the prediction error by weighting based on rough set theory and combining it with the TOPSIS method. However, due to the significant nonlinearity and multi-factor coupling characteristics of rockburst itself, it is still difficult to construct a clear and unified mathematical expression model.

From the perspective of prediction time scale, rockburst prediction can be divided into two categories: short-term prediction and long-term prediction [17,18]. Short-term prediction usually relies on field monitoring methods, such as microseismic monitoring [19,20], electromagnetic radiation monitoring and acoustic emission technology [21–23]. These methods often achieve early warning by capturing the energy release characteristics before rock mass fracture. For example, Zhao et al. [24] proposed a rockburst early warning method that integrates chaotic feature extraction, Transformer prediction, and multi-level feature fusion. Li et al. [25] established a coal–rock stress–electromagnetic radiation coupling model, revealing the control mechanism of loading rate and stress on electromagnetic radiation intensity and time-frequency evolution characteristics. In contrast, long-term prediction is more based on rock mass mechanical properties, geostress environment, and engineering conditions [26–28]. In addition, numerical simulation and experimental research methods are also widely used in rockburst mechanism analysis and prediction research. For example, Papadopoulos et al. [29] constructed a synthetic dataset by integrating undersampling, oversampling, and numerical simulation methods, which effectively alleviated the problems of sample imbalance and insufficient data. Ma et al. [30] established a rockburst prediction model based on key geological structural parameters, providing a new approach for accurate prediction of rockbursts in underground engineering. Liu et al. [31] combined indoor experiments with improved PFC numerical simulation, providing an important basis for the coordinated design of cutting parameters and support in the prevention and control of rockbursts in deep tunnels. Zhang et al. [32] systematically revealed the key role of structural surfaces in controlling the location, intensity, and timing of rockburst occurrence through numerical simulation and engineering examples. In addition, the finite element method, discrete element method, and other methods have made some progress in revealing the rockburst incubation mechanism and disaster evolution law. However, the results of numerical simulation are often affected by factors such as the selection of constitutive models, the setting of boundary conditions, and the accuracy of parameter inversion. Therefore, the relevant research results still have certain limitations when applied to complex engineering sites.

In the context of big data, data-driven machine learning methods have gradually become an important direction for rockburst tendency prediction [33,34]. Table 1 summarizes some existing rockburst prediction models based on different machine learning algorithms and rockburst case datasets. Compared with traditional rockburst classification models, machine learning can automatically mine the nonlinear relationship between multi-source influencing factors and rockburst level from historical engineering samples and has obvious advantages in handling high-dimensional, multi-source, and uncertain data [35]. However, different algorithms still differ in prediction accuracy and engineering applicability, and some high-performance models still have the problem of "black box" operation, which limits their application in rockburst prevention and control decision-making. Therefore, it is necessary to introduce a variety of typical machine learning algorithms to carry out rockburst level comparative prediction and combine sample balancing, parameter optimization, and model interpretation methods to improve the accuracy, stability, and interpretability of rockburst prediction and provide technical support for rockburst risk assessment and safety management in deep underground engineering.

Table 1. Rockburst prediction model developed based on the machine learning algorithms.

Machine Learning Algorithms	Input Parameters	Dataset Size	Author (Year)
BN	σ_θ, σ_c, σ_t, W_{et}	135	Li et al., 2017 [36]
GA-ELM	σ_θ, σ_c, σ_t, W_{et}	30	Li et al., 2017 [37]
CM, NB, RF, KNN	σ_θ, σ_c, σ_t, W_{et}, SCF, B_1	246	Lin et al., 2018 [38]
GA-ENN, GEP, DT, C4.5	σ_θ, σ_c, σ_t, W_{et}	134	Shirani and Taheri, 2019 [39]
DT	σ_θ/σ_c, σ_c/σ_t, We	132	Pu et al., 2018 [40]
C5.0 DT	σ_θ/σ_c, σ_c/σ_t, W_{et}	174	Ghasemi et al., 2020 [41]
PSO-ELM	σ_θ, σ_c, σ_t, σ_θ/σ_c, σ_c/σ_t, W_{et}	344	Xue et al., 2020 [42]
XGBoost, DT, SVM	σ_θ, σ_c, σ_t, W_{et}	134	Shukla et al., 2021 [43]
BOA-SVM	σ_θ/σ_c, σ_c/σ_t, W_{et}	120	Bao et al., 2023 [44]
BO-MLP-RF	σ_θ, σ_c, σ_t, σ_θ/σ_c, σ_c/σ_t, W_{et}	301	Yan et al., 2024 [45]

2. Methodology

2.1. Selection of Rockburst Classification Model

To fully exploit multi-source feature information and improve the accuracy and stability of rockburst classification results, this paper introduces six typical machine learning methods: K-Nearest Neighbors (KNN), Support Vector Machine (SVM), Decision Tree (DT), Random Forest (RF), Multilayer Perceptron Neural Network (MLPNN), and Extreme Gradient Boosting (XGBoost). The schematic diagrams of these six algorithms are shown in Figure 1. Through comparative analysis of the classification performance of different models, the applicability of each method in rockburst classification is systematically evaluated, providing reliable technical support for rockburst prediction and risk assessment.

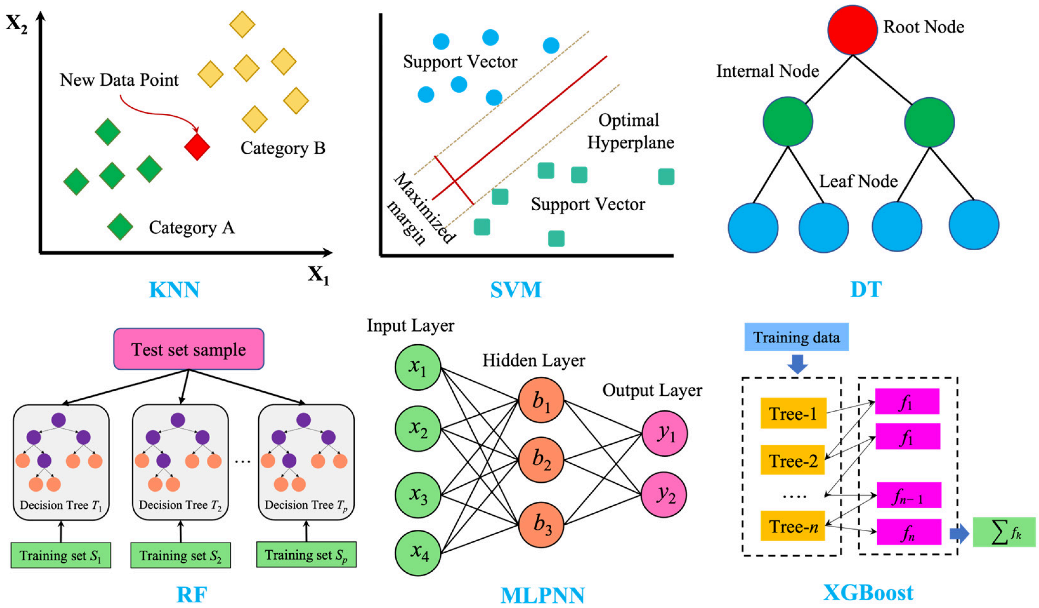

Figure 1. Principle diagrams of these six base learners.

For samples to be classified, KNN [46] calculates its distance to all samples in the training set and selects the K samples with the smallest distance as its neighborhood set, and then determines its category through weighted voting. A Support Vector Machine [47] controls the impact of misclassified samples on the model through a penalty factor, which enhances the generalization ability of the model while ensuring classification accuracy. A Decision Tree [48] is a supervised learning method based on recursive partitioning of feature space. Its modeling process divides the sample into several subsets layer by layer by selecting the optimal partitioning features and thresholds, thereby forming a tree structure. Random Forest [49] adopts the bootstrap sampling method to randomly extract samples from the original dataset to construct training subsets during the training process. At the same time, it randomly selects some features to participate in the optimal partitioning when partitioning at each node, thereby enhancing the diversity of the model. Multilayer Perceptron Neural Networks [50] consist of an input layer, several hidden layers and an output layer. In the rockburst classification problem, this method can fully explore the coupling relationship between various rock mechanical parameters and has a strong expressive ability for complex nonlinear classification tasks. XGBoost [51] is an efficient ensemble learning algorithm based on Gradient Boosting Decision Tree (GBDT). Its core idea is to gradually build multiple weak classifiers in the form of an additive model, so that the newly added model focuses on fitting the residual of the previous model.

Among the above models, KNN and SVMs are often suitable for classification problems under small sample conditions. DTs have strong rule interpretation ability and can be used to extract rockburst level discrimination rules. RF improves the stability and noise resistance of the model through the ensemble strategy. MLPNNs can capture complex nonlinear relationships. XGBoost shows comprehensive advantages in prediction accuracy, generalization ability, and complex feature processing. Considering that rockburst prediction in deep underground engineering has the characteristics of limited sample size, multi-factor coupling, and significant nonlinearity, this paper selects the above six typical classification algorithms for comparative analysis and further combines the Bayesian optimization method to improve the model performance, so as to determine the optimal classification model suitable for rockburst level identification.

2.2. Selection of Evaluation Indicators

To further compare the classification performance of different algorithms in rockburst level identification, this paper selects several commonly used evaluation metrics to quantitatively analyze the model performance, mainly including accuracy, precision, recall, and F1 score [52].

Accuracy measures the overall correctness of the model's predictions, representing the proportion of correctly classified samples out of the total number of samples. In binary classification problems, it can be calculated from true positives (TPs), true negatives (TNs), false positives (FPs), and false negatives (FNs); in multi-class classification problems, accuracy reflects the model's overall classification performance across all samples.

$$\text{Accuracy} = \frac{TP + TN}{TP + FP + TN + FN} \tag{1}$$

Precision primarily evaluates the reliability of model predictions, representing the proportion of samples that are correctly classified into a certain category among all samples predicted as belonging to that category.

$$Precision = \frac{\sum_{l=1}^{L} TP_l}{\sum_{l=1}^{L} (TP_l + FP_l)} \tag{2}$$

where TP_l represents the number of positive samples whose Label is predicted as l and correctly classified, and FP_l represents the number of positive samples whose Label is predicted as l and incorrectly classified.

Recall, on the other hand, focuses on the model's ability to identify real samples, representing the proportion of samples in a certain category that are correctly identified.

$$Recall = \frac{\sum_{l=1}^{L} TP_l}{\sum_{l=1}^{L} (TP_l + FN_l)} \tag{3}$$

where FN_l is the number of samples whose true Label is l but which were assigned to another class.

The F1 score is the harmonic mean of precision and recall, comprehensively reflecting the model's performance in both precision and recall. Its value ranges from 0 to 1, with a higher value indicating better model performance.

$$F1 - score = 2 \times \frac{Precision \cdot Recall}{Precision + Recall} \tag{4}$$

In multi-class classification tasks, the aforementioned metrics can typically be calculated using either the macro average or weighted average. Macro average calculates the metric for each category separately and then takes the arithmetic mean, unaffected by the number of samples in each category. Weighted average, on the other hand, weights the samples according to their respective number of samples. Since this paper balances samples of different rockburst levels using oversampling, ensuring equal importance for each category, macro average is used to evaluate the model's classification performance.

3. Description and Preprocessing of the Dataset

3.1. Description of the Dataset

The classification accuracy of rockburst type identification models usually depends on sufficient and reliable training samples. This paper systematically reviews and summarizes relevant data from references [53] and finally selects 357 sets of rockburst sample data. The data includes projects such as underground hydroelectric caverns, deep-buried tunnels, and mine roadways. According to the degree of damage and characteristics of rockbursts, the samples are divided into four levels: none rockburst, light rockburst, moderate rockburst, and strong rockburst, corresponding to levels 0, 1, 2, and 3, respectively. Based on the above classification criteria, the level distribution of the sample data is statistically analyzed, and a schematic diagram of the sample number distribution is drawn, as shown in Figure 2. The statistical results show that there were 55 groups with "none rockburst," representing approximately 15.41% of the total sample; 103 sets of samples experienced light rockburst, accounting for approximately 28.85%; the largest number of samples experienced moderate rockburst, totaling 133 sets, accounting for 37.25% of the total; and 66 sets of samples experienced strong rockburst, accounting for approximately 18.49%. The descriptions and classification standards for each rockburst level are shown in Table 2.

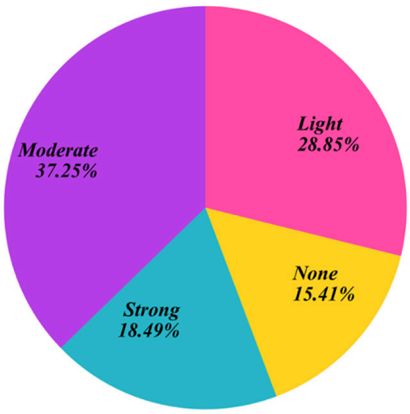

Figure 2. Distribution of the different rockburst levels.

This paper constructs a characteristic system for judging rockburst levels from multiple perspectives, including stress conditions, rock strength characteristics, and energy and brittleness features. Six representative parameters are selected as model input variables. These characteristic parameters include: maximum tangential stress of the surrounding rock (σ_θ), reflecting the degree of stress concentration in the engineering environment; uniaxial compressive strength (σ_c) and uniaxial tensile strength (σ_t), characterizing the mechanical bearing capacity of the rock itself; rock elastic energy index (W_{et}), depicting the energy accumulation and release potential of the rock mass during loading; and two comprehensive indices—stress coefficient (σ_θ/σ_c) and rock brittleness coefficient (σ_c/σ_t)—are introduced to reflect the relationship between stress level and rock strength and brittleness.

The distribution characteristics of the six characteristic parameters in Figure 3 under different rockburst levels show that, as the rockburst intensity increases, the indicators generally exhibit a pattern of migration from low to high values and expansion from concentration to dispersion. On the other hand, the distribution of the characteristic indicators across different rockburst levels is not balanced. Low-level rockburst samples are mostly concentrated in the low-value region of the indicators, while medium- and strong-intensity rockburst samples dominate the high-value region. Especially in parameters such as maximum tangential stress, elastic energy index, and stress coefficient, high-level rockburst samples exhibit obvious "long tail" and high dispersion characteristics, leading to significant differences in distribution between levels. This imbalance of indicators places higher demands on the feature weight allocation and model robustness of subsequent rockburst level discrimination algorithms.

Table 2. Criteria for determining the severity of rockburst.

Rockburst Level	Description	Project Impact
None rockburst	During the excavation process, the surrounding rock remained basically stable, with no obvious noise, spalling, peeling, or rock fragment ejection.	It has virtually no impact on construction.
Light rockburst	The surrounding rock showed minor cracks, accompanied by cracking or slight popping sounds; small rock fragments peeled off and flaked off in some areas.	The impact on the support structure is relatively small and can generally be controlled by strengthening monitoring and local support.
Moderate rockburst	The elastic energy accumulated inside the rock mass was rapidly released, producing a distinct cracking sound; the surrounding rock underwent extensive fracturing and spalling.	It poses an obvious threat to construction safety and requires strengthened support and protective measures.
Strong rockburst	The attack is sudden and accompanied by loud noises and strong vibrations; a large number of rock fragments are ejected at high speed, causing serious damage to the surrounding rock.	It can cause casualties, equipment damage, and serious engineering accidents.

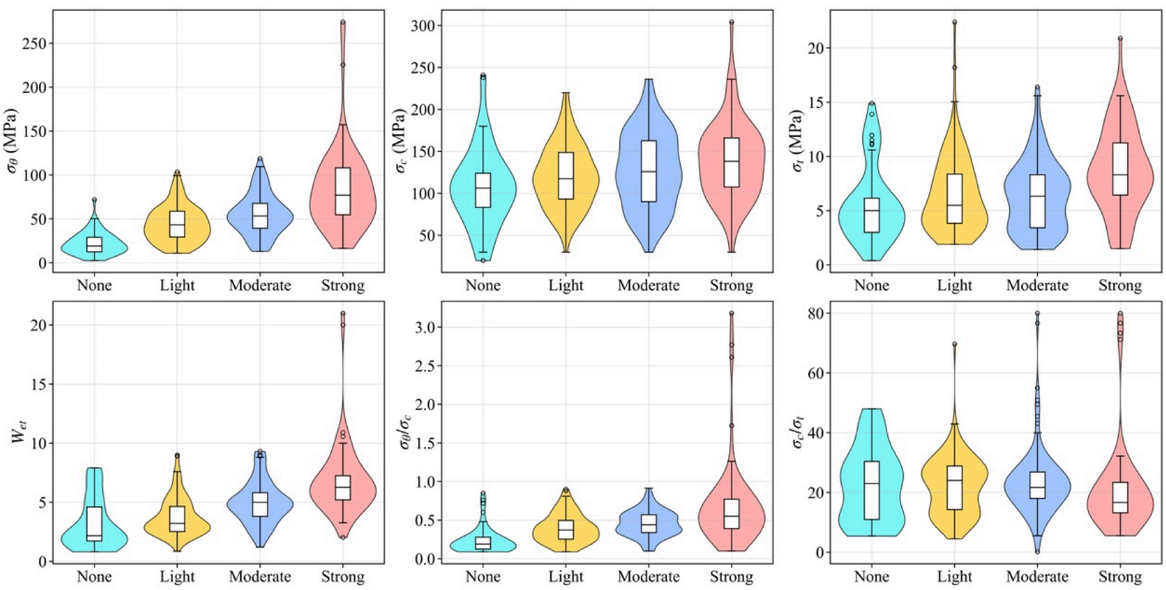

Figure 3. Violin plots of the dataset.

Figure 4 illustrates the correlations among the six characteristic parameters. Overall, there are varying degrees of correlation among the parameters, but no severe multicollinearity is observed. The maximum tangential stress and stress coefficient exhibit the strongest positive correlation, with a correlation coefficient of 0.82. σ_θ also shows a certain positive correlation with the elastic energy index, with a correlation coefficient of 0.45, indicating that higher tangential stress is beneficial to the accumulation of elastic energy within the rock mass and is one of the important mechanical conditions in the rockburst incubation process. The correlation coefficient between the uniaxial compressive strength and the uniaxial tensile strength is 0.47. Meanwhile, the correlation coefficients between σ_c and W_{et} are 0.43, and between σ_c and σ_θ/σ_c are -0.21, indicating a certain connection between compressive strength and energy accumulation and stress coefficient, but the correlation is not strong. Regarding brittleness-related indicators, the rock brittleness coefficient and the uniaxial tensile strength show a strong negative correlation, with a correlation coefficient of -0.64. In contrast, σ_c/σ_t shows relatively weak correlation with other feature parameters, indicating that the brittleness coefficient is highly independent within the feature system. Overall, the six feature parameters reflect rockburst occurrence conditions from aspects such as stress level, rock strength, energy accumulation, and brittleness characteristics. Although some parameters exhibit certain correlations, particularly σ_θ and σ_θ/σ_c, and σ_t and σ_c/σ_t, the overall correlation coefficients do not reach a high level of redundancy. This suggests that the selected features do not suffer from severe multicollinearity and can provide comprehensive and complementary input information for subsequent rockburst severity prediction models.

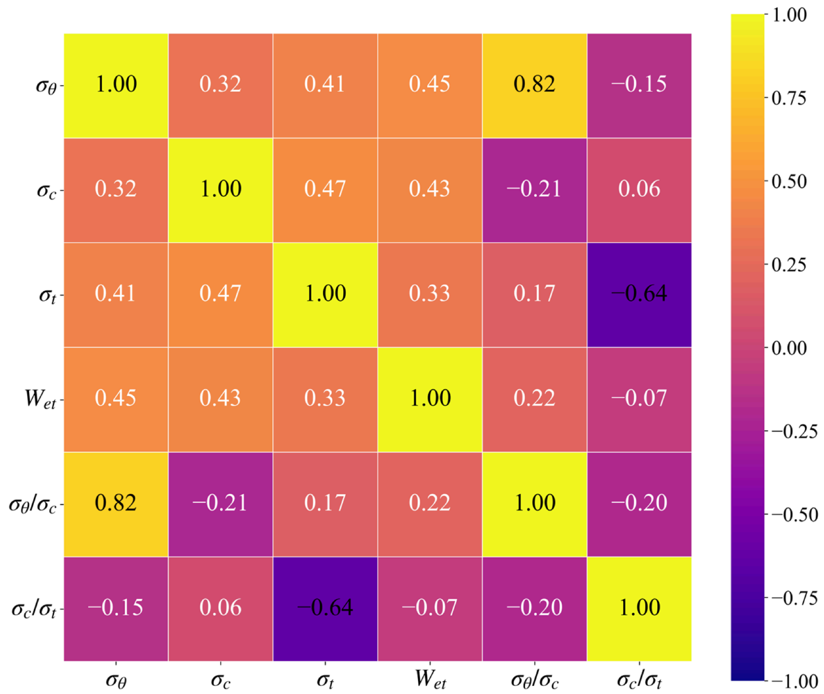

Figure 4. Correlation coefficients of various indicators.

Furthermore, the correlation between σ_c/σ_t and other indices is generally weak, suggesting that the brittleness coefficient has strong independence within the characteristic system, which helps improve the model's ability to identify differences in rockburst intensity. Comprehensive analysis shows that there is no serious multicollinearity problem among the six characteristic parameters, and they all demonstrate different emphases in their information contributions regarding stress, energy, strength, and brittleness.

By combining the scatter plots of various indicators (Figure 5), the distribution characteristics of each indicator can be observed from multiple dimensions. First, the histogram distribution on the diagonal shows that most parameters have dense samples in the low-value range, while the samples are relatively sparse in the high-value range. This distribution pattern indicates that extreme stress, energy, or stress coefficient conditions occur less frequently, but often correspond to higher intensity rockburst levels. Second, low-level samples (none rockburst and moderate rockburst) are mostly concentrated in the core area of the feature space, with dense point clouds and a high degree of overlap; while medium-intensity and strong rockburst samples gradually expand outward and into the high-value area, forming a clearer boundary outline. In addition, multiple feature combinations show potential advantages in distinguishing rockburst levels. For example, when stress or energy-related indicators are combined with strength or brittleness indicators, high-level rockburst samples are more likely to be distributed in specific areas of two-dimensional space, while low-level samples are less likely to appear in these areas. Furthermore, a small number of outliers can still be seen in the scatter plot distribution, mainly appearing in high-level rockburst samples, reflecting the complexity and uncertainty of the rockburst generation mechanism under actual engineering conditions.

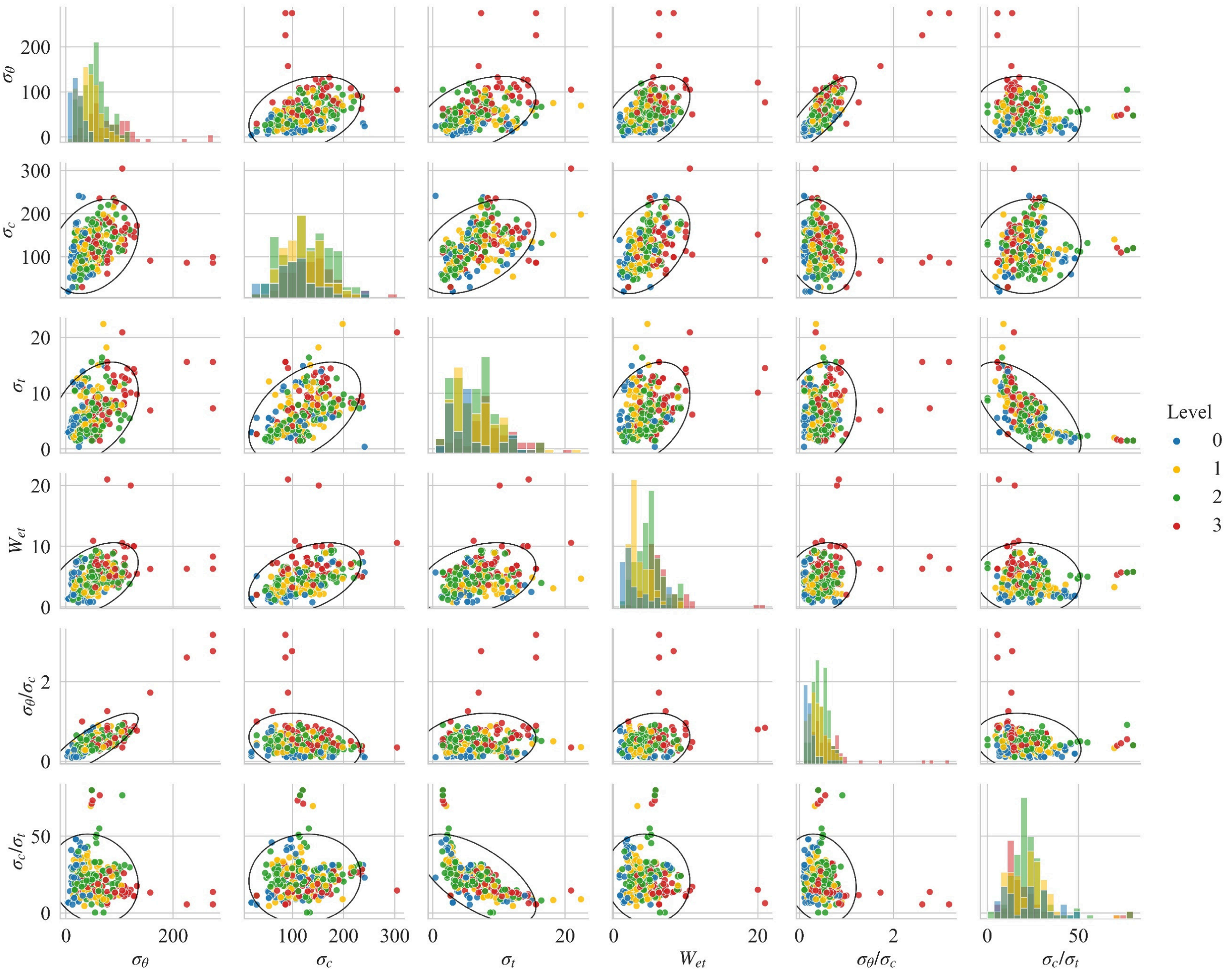

Figure 5. Scatter plots and statistical distributions of each indicator.

Against this backdrop, it is essential to introduce oversampling methods to balance the data. By expanding the minority class samples, the density of medium-intensity and strong rockburst samples in high-dimensional space can be enhanced, allowing them to form a more continuous and complete clustering structure in the joint distribution of multiple features. Simultaneously, data balancing can also reduce the model's sensitivity to local outliers to some extent. By increasing the representativeness of minority class samples in the feature space, the model no longer overly relies on individual extreme points to characterize high-intensity rockburst features during training, thereby improving the stability and generalization ability of the overall classification results.

3.2. Preprocessing of Raw Data

In cases of unbalanced sample distribution, the traditional simple replication of minority class samples is prone to model overfitting and is difficult to realistically depict the distribution structure of different class samples in the feature space. To this end, this paper further introduces the SMOTE (Synthetic Minority Over-sampling Technique) oversampling method [54] to synthesize and expand minority class samples, thereby improving the balance of data distribution. The basic principle of SMOTE can be intuitively understood by referring to Figure 6: In the original sample space, different class samples are discretely distributed, among which the minority class samples (Class B samples in the figure) are few in number and the distribution area is relatively isolated. SMOTE does not simply repeat the existing minority class samples, but takes a certain minority class sample as the benchmark, finds several nearest neighbor samples of the same class in its feature space, and then generates new synthetic sample points in the direction of the line connecting the sample and its neighboring samples through linear interpolation. The newly added polygonal samples on the right side of the figure represent the synthetic samples obtained by this interpolation method, which are distributed among the original minority class samples. In this way, SMOTE effectively fills in the "gap regions" between minority class samples, avoiding the sample overlap problem caused by simple duplication, while enhancing the representativeness of the minority class in the feature space.

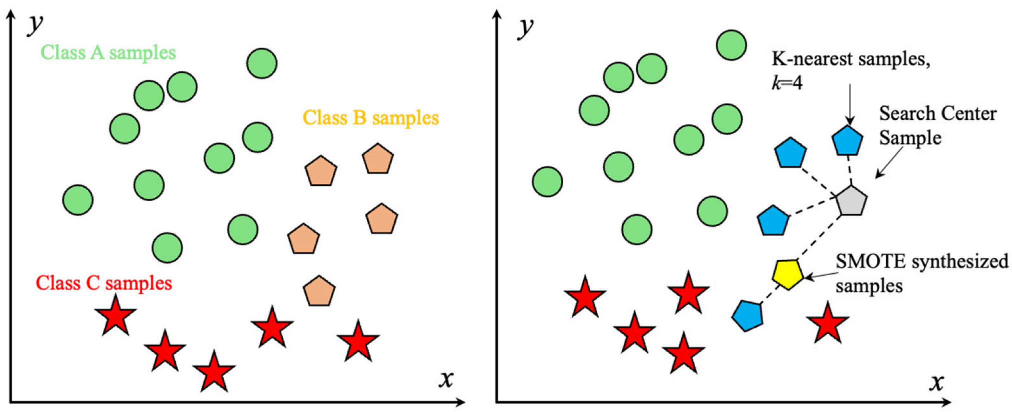

Figure 6. The basic principle of SMOTE oversampling.

To further verify the effect of SMOTE oversampling on improving the distribution structure of minority class samples in the feature space, this paper compares and analyzes the distribution of the original data and the samples processed by SMOTE. Compared with the original data, the samples generated by SMOTE can expand better along the original minority class sample distribution direction in most feature dimensions, making the distribution in the feature space more continuous and smoother. SMOTE does not destroy the statistical characteristics of the original data, but enhances the expressive power of minority class samples in the multi-dimensional feature space while maintaining the consistency of the distribution shape, providing a more reasonable data foundation for the stable training and generalization performance improvement of the subsequent classification model.

4. Rockburst Tendency Classification Model

4.1. Analysis Flow of Rockburst Classification Algorithm

Rockburst is a complex dynamic disaster influenced by multiple factors, including stress environment, rock mechanical properties, and energy evolution. Single indicators or empirical criteria are insufficient to comprehensively reflect the differences in rockburst intensity. Therefore, it is necessary to utilize multi-feature-driven machine learning methods for quantitative identification and comprehensive judgment of rockburst levels. The specific steps are as follows, and the flowchart is shown in Figure 7.

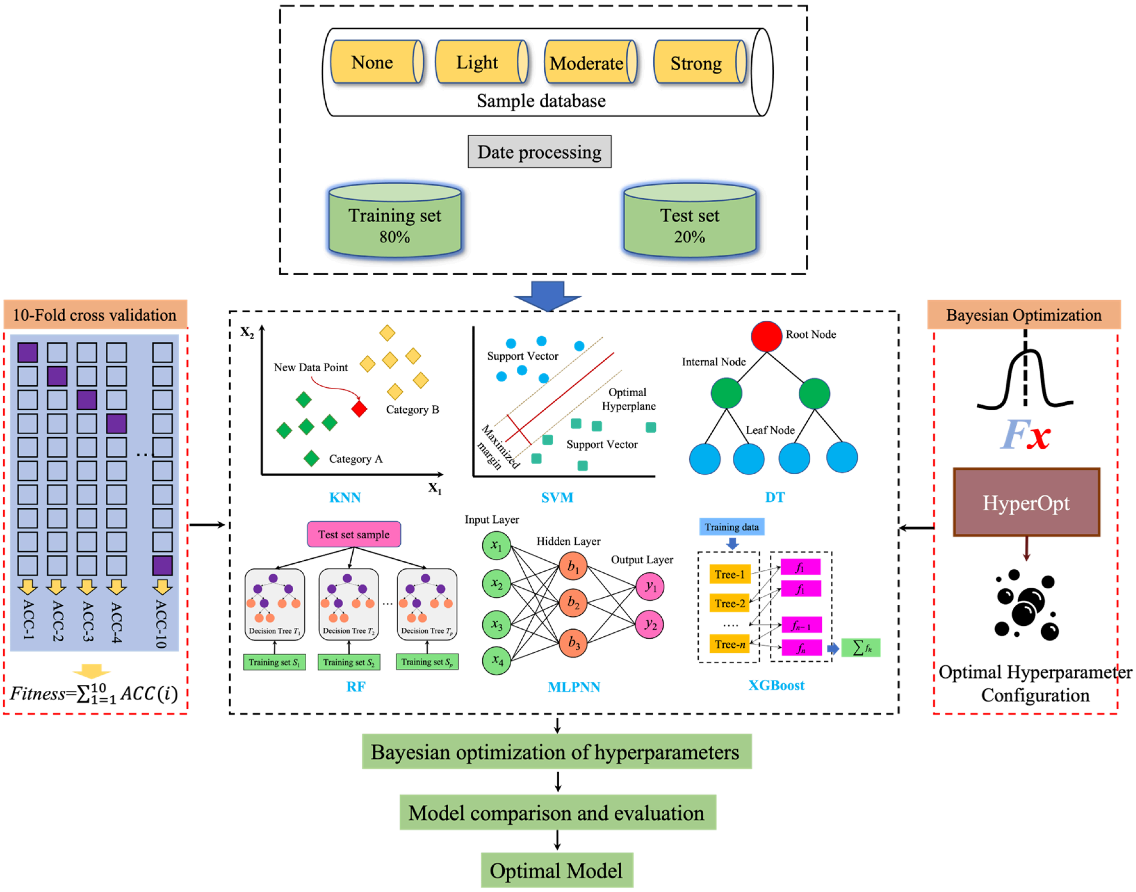

Figure 7. Flowchart of the proposed approach.

Step 1: Sample construction and feature selection. First, collect and organize rockburst samples from existing engineering examples and literature. Based on this, select representative feature indicators from aspects such as stress conditions, rock strength characteristics, and energy and brittleness characteristics to construct the input feature system for the rockburst classification model.

Step 2: Data preprocessing and sample balancing. Considering the imbalance in the number of samples for different rockburst levels, an oversampling method is used to expand the minority class samples.

Step 3: Training and test set splitting. The preprocessed dataset is divided into training and test sets according to a certain ratio, with the training set accounting for 80% and the test set accounting for 20%.

Step 4: Model construction and training. Multiple rockburst classification models are constructed on the training set and trained using ten-fold cross-validation. Cross-validation can fully utilize limited sample data, effectively reduce the random errors caused by random partitioning, and thus obtain more stable model performance evaluation results.

Step 5: Hyperparameter optimization. To further improve model performance, a Bayesian optimization method is introduced to automatically search for model hyperparameters. By iteratively updating the parameter space, the optimal parameter combination is obtained, allowing the classification model to achieve its best performance on the training set.

Step 6: Model evaluation and comparative analysis. The classification results of each model are evaluated using the test set. Evaluation metrics such as accuracy, precision, recall, and F1 score are employed to compare and analyze different models in terms of overall performance and the ability to identify each category, comprehensively judging their merits.

Step 7: Determination and discussion of the optimal model. Considering the classification performance and stability of the models on the test set, the best-performing rockburst classification model is selected as the final result for rockburst level discrimination analysis. This model can provide reliable technical support for the identification and prevention of rockburst risks in engineering practice.

4.2. Determination of Hyperparameters

Hyperparameters are parameters that need to be manually set before model training begins. They are mainly used to control the model structure or learning process. Their values are not directly learned from training data but are configured based on the specific task and dataset. Common optimization methods for determining hyperparameters include grid search, random search, and Bayesian optimization. Grid search relies on a pre-defined search range and step size, requiring extensive model training when the model contains multiple hyperparameters or has a large parameter value space. Random search reduces the number of parameter combinations traversed through random sampling, offering advantages in high-dimensional parameter spaces; however, each sample is independent, making it difficult to effectively guide subsequent search directions. Evolutionary algorithms (such as genetic algorithms) optimize parameters by simulating natural selection, crossover, and mutation processes, possessing strong global search capabilities and handling complex nonlinear optimization problems. However, these methods typically require large population sizes and multiple iterations, increasing computational burden when model training costs are already high. In contrast, Bayesian optimization can more efficiently approximate the optimal parameter solution with a limited number of evaluations, making it more suitable for optimization problems involving complex models and high-dimensional parameter spaces. Therefore, this paper chooses Bayesian optimization to optimize the model's hyperparameters.

Bayesian optimization is a global optimization strategy oriented towards a black-box objective function. Its core idea is to use a probabilistic model to characterize the latent distribution characteristics of the objective function during the optimization process. This method first constructs a prior model of the objective function based on existing samples (usually using a Gaussian process). Then, it continuously updates the posterior distribution by incorporating newly acquired observations. By using a sampling function to achieve a balance between "exploration" and "utilization," it gradually determines the next set of most promising parameter values. Through continuous iterative updates to the model and sampling points, an approximate optimal solution to the objective function is finally obtained. The hyperparameter selection and optimal values for the six algorithms are shown in Table 3.

Table 3. Hyperparameter selection and optimal values for six algorithms.

ML Algorithms	Hyperparameters	Scope of Values	Optimal Values
KNN	n_neighbors	(1, 10)	3
SVM	Penalty coefficient C gamma	(0.001, 10) (0.001, 1)	5.05 0.44

Table 3. *Cont.*

ML Algorithms	Hyperparameters	Scope of Values	Optimal Values
DT	max_depth min_samples_split min_samples_leaf	(1, 10) (2, 10) (1, 10)	7 6 2
RF	n_estimators max_depth min_samples_split	(10, 300) (10, 100) (2, 10)	46 10 7
MLPNN	hidden_layer_sizes activation	(1, 20) (100, 1000)	12 964
XGBoost	n_estimators max_depth learning_rate subsample reg_alpha reg_lambda	(10, 300) (1, 10) (0.001, 1) (0.1, 1) (0.1, 1) (0.1, 1)	284 4 0.2 0.5 0.3 0.8

5. Discussions

5.1. Confusion Matrices and Results of Each Model on Test Set

From the overall distribution of the confusion matrix, as shown in Figure 8, the algorithms generally outperformed the intermediate levels in identifying none rockburst (level 0) and strong rockburst (level 3). Most models' predictions for level 0 samples were concentrated on the diagonal, with few misclassifications, indicating strong separability of none rockburst samples in the feature space. Similarly, the identification accuracy for strong rockburst samples was high, with only a small number misclassified as moderate rockburst (level 2), suggesting that high-intensity rockbursts have prominent characteristics in terms of stress, energy, and brittleness. In contrast, the confusion between light rockburst (level 1) and moderate rockburst (level 2) was more pronounced, with some samples misclassifying between the two classes, reflecting a certain overlap in the feature distribution of these two levels, which is also a major challenge in rockburst level discrimination.

The quantitative evaluation results show significant differences in classification performance among different models (Table 4). The BO-XGBoost model performed best, achieving an accuracy of 0.7664, a macro-P of 0.7664, and a macro-F1 of 0.7662. This indicates that the model not only has high overall classification accuracy but also exhibits relatively balanced recognition capabilities across different rockburst levels, demonstrating strong consistency and stability. BO-RF performed second best, with an accuracy and macro-F1 of 0.7290 and 0.7281, respectively, showing good classification stability, but still lagging behind BO-XGBoost. BO-KNN and BO-SVM performed at a moderate level, with accuracies of 0.7009 and 0.7103, respectively. Their macro-average indicators were quite similar, indicating that they possessed some recognition ability for each category after balancing, but their overall stability was lower than that of the ensemble model. In comparison, BO-DT and BO-MLPNN performed relatively poorly in classification, with accuracies of 0.6636 and 0.6822, respectively. The misclassification of intermediate-level samples in the confusion matrix was particularly prominent, indicating that single decision structures or shallow neural networks have certain limitations in characterizing the complex nonlinear features of rockbursts.

https://doi.org/10.3390/pr14152450

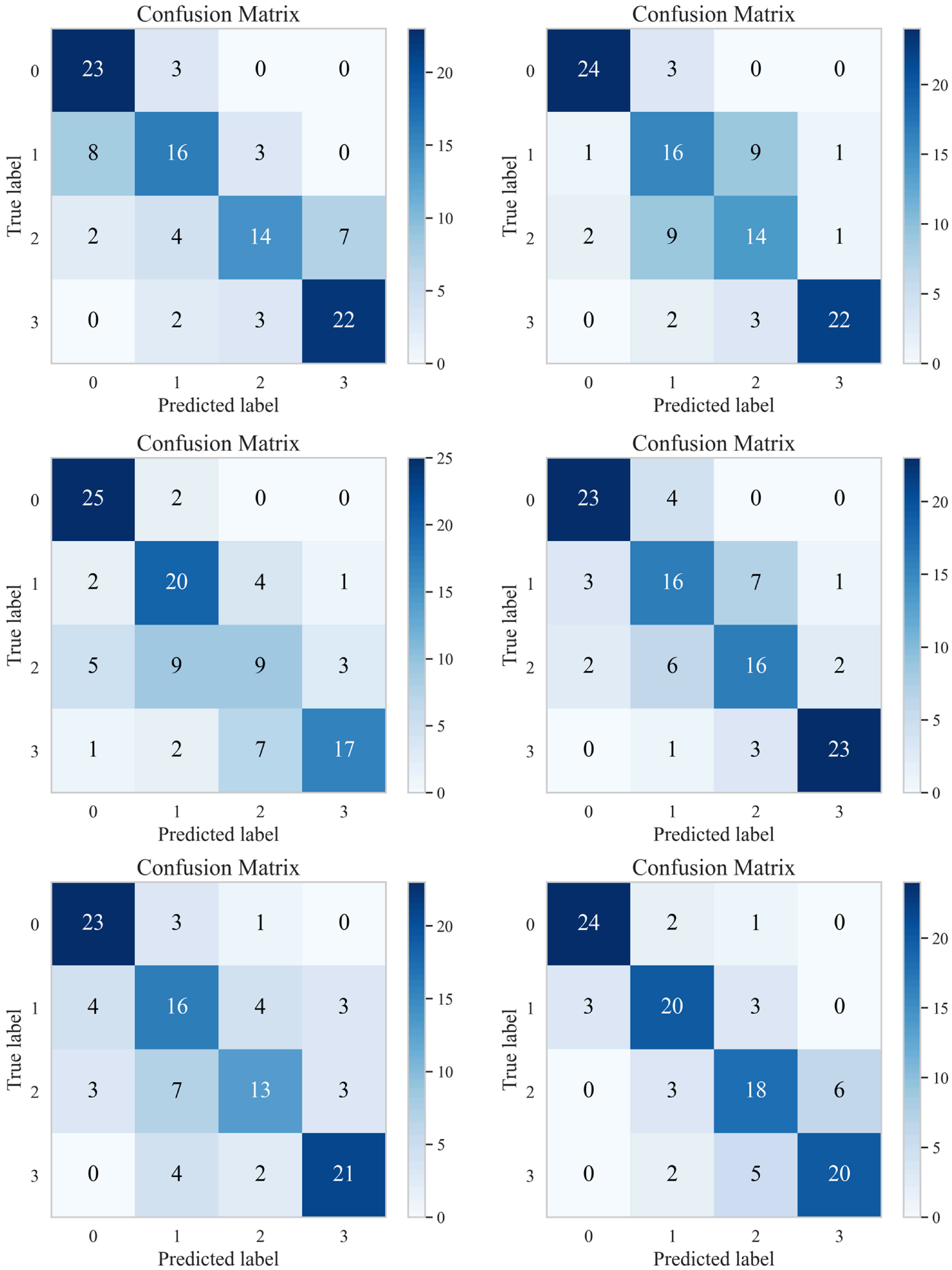

Figure 8. Confusion matrices of each model on test set.

Table 4. The quantitative evaluation results of six models.

ML Algorithms	Accuracy	Macro-P	Macro-R	Macro-F1
BO-KNN	0.7009	0.6989	0.7026	0.6941
BO-SVM	0.7103	0.7193	0.7087	0.7129
BO-DT	0.6636	0.6558	0.6606	0.6499
BO-RF	0.7290	0.7285	0.7279	0.7281
BO-MLPNN	0.6822	0.6819	0.6807	0.6779
BO-XGBoost	0.7664	0.7664	0.7664	0.7662

Analysis of the confusion matrix and evaluation metrics reveals that the Bayesian-optimized ensemble learning models demonstrate significant advantages in rockburst classification, particularly BO-XGBoost and BO-RF, which maintain high overall accuracy while exhibiting good recognition capabilities for each rockburst level. Among these, BO-XGBoost achieves the best results in accuracy, macro-average precision, and macro-average F1 score, making it the preferred model for rockburst classification in this paper and providing more reliable technical support for rockburst risk identification and level determination in engineering practice.

5.2. Hyperparameters Tuning Process

Taking the BO-XGBoost model as an example, the iterative results of its hyperparameter optimization process are analyzed, as shown in Figure 9. The figure shows the change trajectory of the key hyperparameters of XGBoost during 200 optimization iterations. Overall, each hyperparameter showed significant fluctuations in the early stages of iteration, indicating that the optimization algorithm conducted a thorough search within a wide parameter space to explore the impact of different parameter combinations on model performance. Specifically, n_estimators showed large fluctuations in the early stages, with values fluctuating frequently within a wide range; as the number of iterations increased, its values gradually concentrated around 180–230, with a few still showing relatively high values in the later stages, indicating that the model's search for the number of trees gradually stabilized. max_depth fluctuated significantly in the early stages and then mainly concentrated in the range of 7–9, indicating that a deeper tree structure is more conducive to characterizing the complex nonlinear relationship between rockburst level and input features. learning_rate showed a trend of concentrating from a large range of searches to a smaller value range in logarithmic coordinates and mainly stabilized around 10^{-2} in the later stages, indicating that a smaller learning rate helps improve the stability of the model training process. Regarding the regularization parameter, 'reg_alpha' remained highly volatile throughout the iterations, indicating that the impact of L1 regularization strength on model performance is complex, and the optimization process did not show a clear monotonic convergence trend. In contrast, 'reg_lambda' gradually concentrated around 0.35–0.40 in the mid-to-late stages, suggesting that moderate L2 regularization helps control model complexity and improve generalization ability. Furthermore, 'subsample' fluctuated significantly in the early stages, then generally decreased and gradually stabilized in the range of approximately 0.30–0.40, indicating that under the current dataset conditions, moderately reducing the sample sampling ratio can enhance the randomness of the model, thereby improving its generalization performance. Overall, the hyperparameter optimization process of BO-XGBoost went through a process of extensive exploration in the early stages to local stability in the later stages, demonstrating that the optimization algorithm can effectively search for optimal parameter regions and support the improvement of model performance.

Comprehensive analysis shows that by combining Bayesian optimization and cross-validation, the BO-XGBoost model can quickly obtain a high-performance and stable combination of hyperparameters within a limited number of iterations, providing a reliable model configuration basis for subsequent rockburst level classification and further demonstrating the rationality and effectiveness of the hyperparameter optimization strategy adopted in this paper.

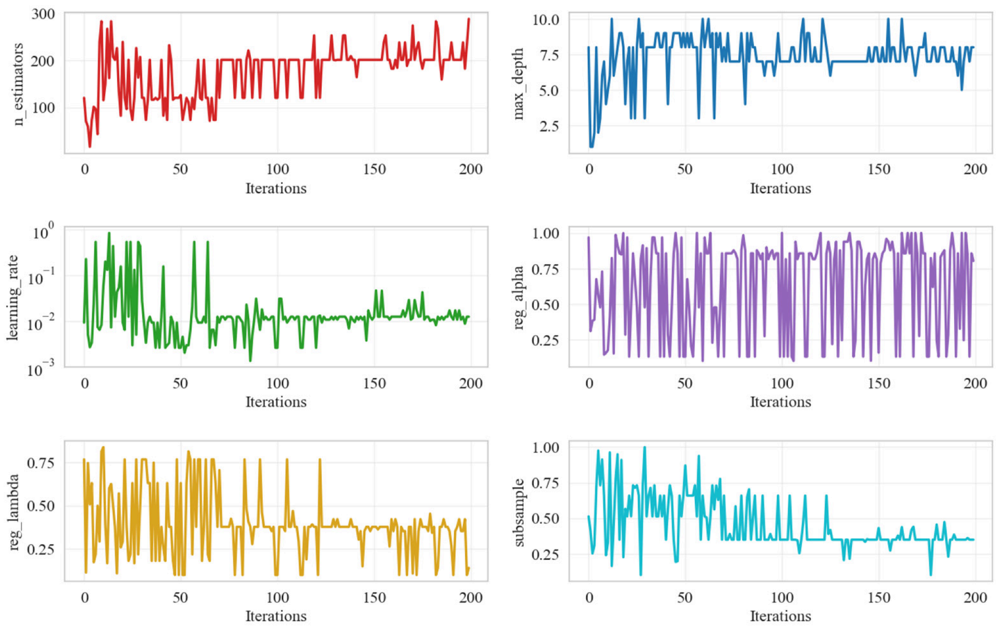

Figure 9. Hyperparameter tuning process of XGBoost model.

5.3. Evaluation and Comparison of Six Classifiers

To further evaluate the performance of different rockburst classification models from the perspective of probabilistic discriminative ability, this paper plots the ROC curves of BO-KNN, BO-SVM, BO-DT, BO-RF, BO-MLPNN, and BO-XGBoost under a multi-classification task and calculates the micro-average AUC value for each rockburst level, as shown in Figure 10. The closer the AUC value is to 1, the stronger the model's ability to distinguish samples of different rockburst levels; the closer the ROC curve is to the upper left corner, the better the model's overall classification performance.

From the overall results, the ROC curves of all six models are significantly higher than the random classification baseline, indicating that each model has a certain ability to identify rockburst levels, but there are still differences in discriminative performance among different models. Among them, BO-XGBoost has the best overall performance, with a micro-average AUC of 0.9351, significantly higher than the other models, indicating that it has the strongest overall discriminative ability across the four rockburst levels. The micro-average AUC of BO-RF is 0.9090, second only to BO-XGBoost, indicating that the random forest model also has good stability and generalization ability within the ensemble learning framework. In contrast, the micro-average AUCs of BO-KNN, BO-DT, and BO-MLPNN are 0.8612, 0.8619, and 0.8690, respectively, showing relatively weak overall discriminative ability; the micro-average AUC of BO-SVM is 0.8891, at a moderate level.

From the AUC results for different rockburst levels, all six models generally have strong recognition ability for non-rockburst samples (Class 0), with AUC values all above 0.92. Among them, BO-XGBoost achieves the most outstanding performance with an AUC of 0.9894 for Class 0, indicating that this model can accurately distinguish non-rockburst samples from other levels of samples. For strong rockburst samples (Class 3), all models demonstrated good discriminative ability. The AUCs of BO-SVM, BO-RF, and BO-XGBoost reached 0.9523, 0.9676, and 0.9370, respectively, indicating that strong rockburst samples have significant distinguishing features in the feature space, and the models can easily capture their discrimination boundaries. In contrast, the identification of light rockburst (Class 1) and moderate rockburst (Class 2) is relatively more difficult. The AUCs of models such as BO-KNN, BO-SVM, and BO-MLPNN for Class 1 and Class 2 are mostly around 0.76–0.80, indicating some feature overlap between these two classes and relatively limited model discriminative ability. BO-DT's AUC for Class 2 is only 0.7106, indicating that a single decision tree model is significantly insufficient in identifying moderate rockburst. After integrating multiple decision trees, BO-RF improved the AUC for Class 2 to 0.8248, indicating that the ensemble strategy can improve the discrimination performance of intermediate-level rockburst to some extent. BO-XGBoost achieved AUCs of 0.9361 and 0.8442 for Class 1 and Class 2, respectively, both outperforming most comparative models, demonstrating its stronger ability to distinguish between light and moderate rockburst samples.

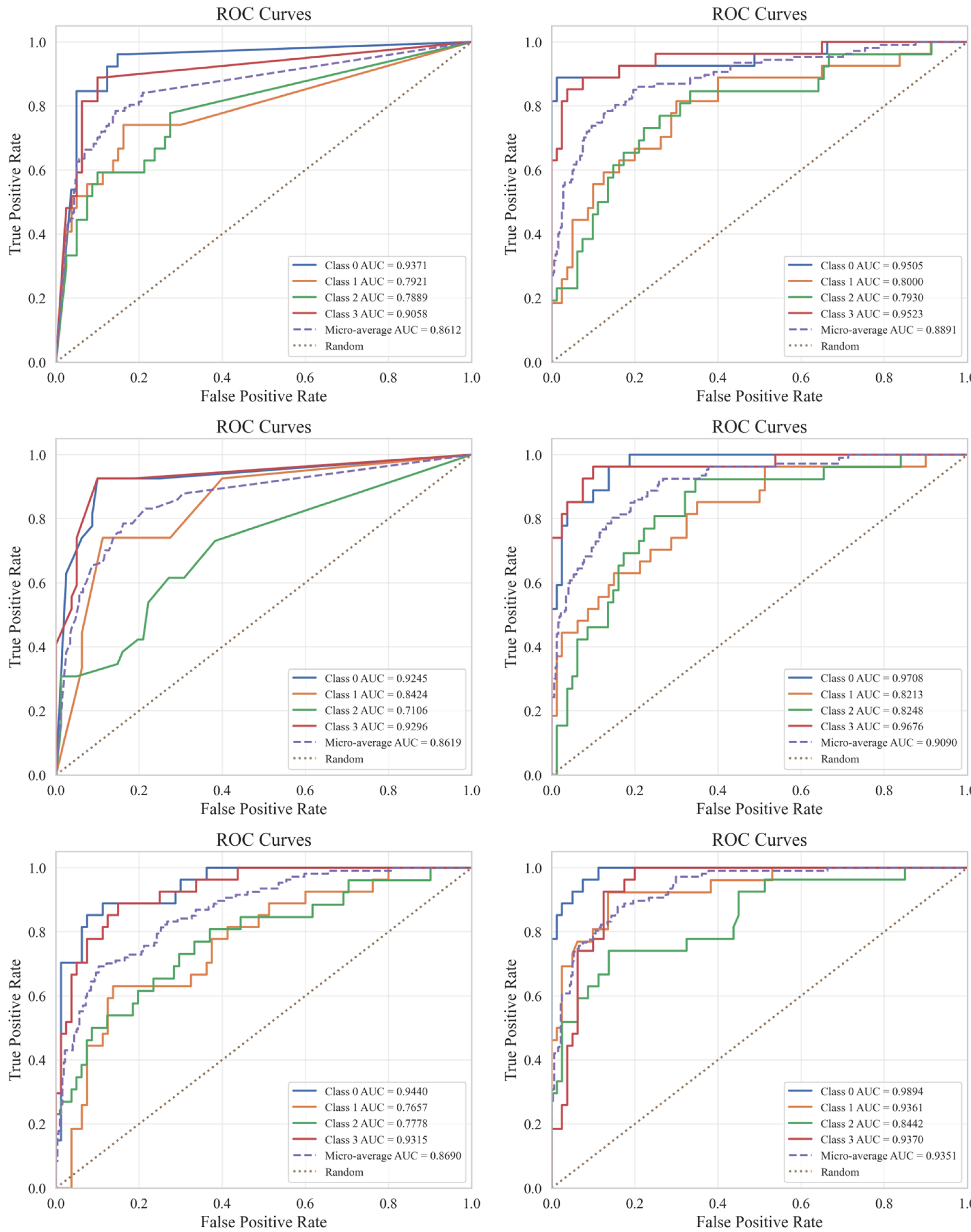

Figure 10. ROC curves and AUC values of six classifiers.

Overall, BO-XGBoost maintained high AUC values across all rockburst levels, showing a significant advantage in Class 0 and Class 1 identification. Furthermore, its micro-average AUC was the highest, indicating that the model can effectively identify samples with clear boundary features, such as none rockburst and strong rockburst, and also distinguish easily confused categories such as light and moderate rockburst. In comparison, BO-

KNN, BO-DT, and BO-MLPNN have certain shortcomings in identifying intermediate-level samples. While BO-SVM and BO-RF have better overall performance, their comprehensive discriminative ability is still lower than that of BO-XGBoost. Therefore, BO-XGBoost demonstrates superior probabilistic discriminative ability, class differentiation ability, and overall generalization performance in the multi-class prediction task of rockburst level.

5.4. SHAP-Based Model Interpretability Analysis

To further reveal the decision-making mechanism of the BO-XGBoost model in the rockburst level discrimination process, this paper introduces the SHAP (Shapley Additive Explanations) method to analyze the interpretability of the model output, as shown in Figure 11. The SHAP value quantitatively characterizes the direction and intensity of each input variable's contribution to the prediction result of a specific rockburst level: a positive SHAP value indicates that the feature value drives the model towards the corresponding rockburst level, while a negative SHAP value indicates that it inhibits the model's discrimination of that level; the larger the absolute value, the more significant the influence of the feature on the model output.

From the global SHAP feature importance results, it can be seen that the contributions of the six input parameters to the discrimination results of the BO-XGBoost model are significantly different, as shown in Figure 12. Among them, the elastic energy index (W_{et}) has the highest contribution, accounting for 25.75% of the SHAP importance, indicating that it is the primary controlling factor affecting rockburst level discrimination. Secondly, the stress coefficient σ_θ/σ_c accounting for 22.68% of the importance indicates that the stress concentration of the surrounding rock also plays a crucial role in the model's decision-making. The brittleness coefficients σ_c/σ_t, maximum tangential stress σ_θ, uniaxial tensile strength σ_t, and uniaxial compressive strength σ_c account for 16.15%, 14.42%, 10.92%, and 10.08% of the importance, respectively. Overall, the model's determination of rockburst severity is mainly controlled by the energy accumulation state, stress concentration, and rock brittleness characteristics. Among these, W_{et}, σ_θ/σ_c, and σ_c/σ_t contribute over 60% cumulatively and are the core input variables for the BO-XGBoost model in identifying rockburst severity.

The SHAP distributions for different rockburst levels further reveal a clear level-dependent contribution direction for each feature. For Level 0 (none rockburst), high values of σ_θ/σ_c and W_{et} are mostly distributed in the negative SHAP region, while low-value samples are more likely to appear in the positive SHAP region, indicating that low stress concentration and low energy accumulation are more conducive to the model's classification as none rockburst. As σ_θ/σ_c and W_{et} increases, the model's support for the no-rockburst level weakens significantly. This result is consistent with the physical mechanism that rockburst generation requires a certain stress reserve and energy accumulation.

For Level 1 (moderate rockburst), W_{et} still exhibits the widest SHAP distribution range, indicating its strong influence on the classification of moderate rockburst. In the figure, samples with lower W_{et} are more likely to produce positive SHAP contributions, while higher W_{et} mostly show negative contributions, indicating that moderate rockbursts typically correspond to relatively limited energy release levels. Meanwhile, the other features are mainly concentrated near zero, indicating that the discrimination of moderate rockbursts is not dominated by a single parameter, but is influenced by the coupling of multiple factors.

https://doi.org/10.3390/pr14152450

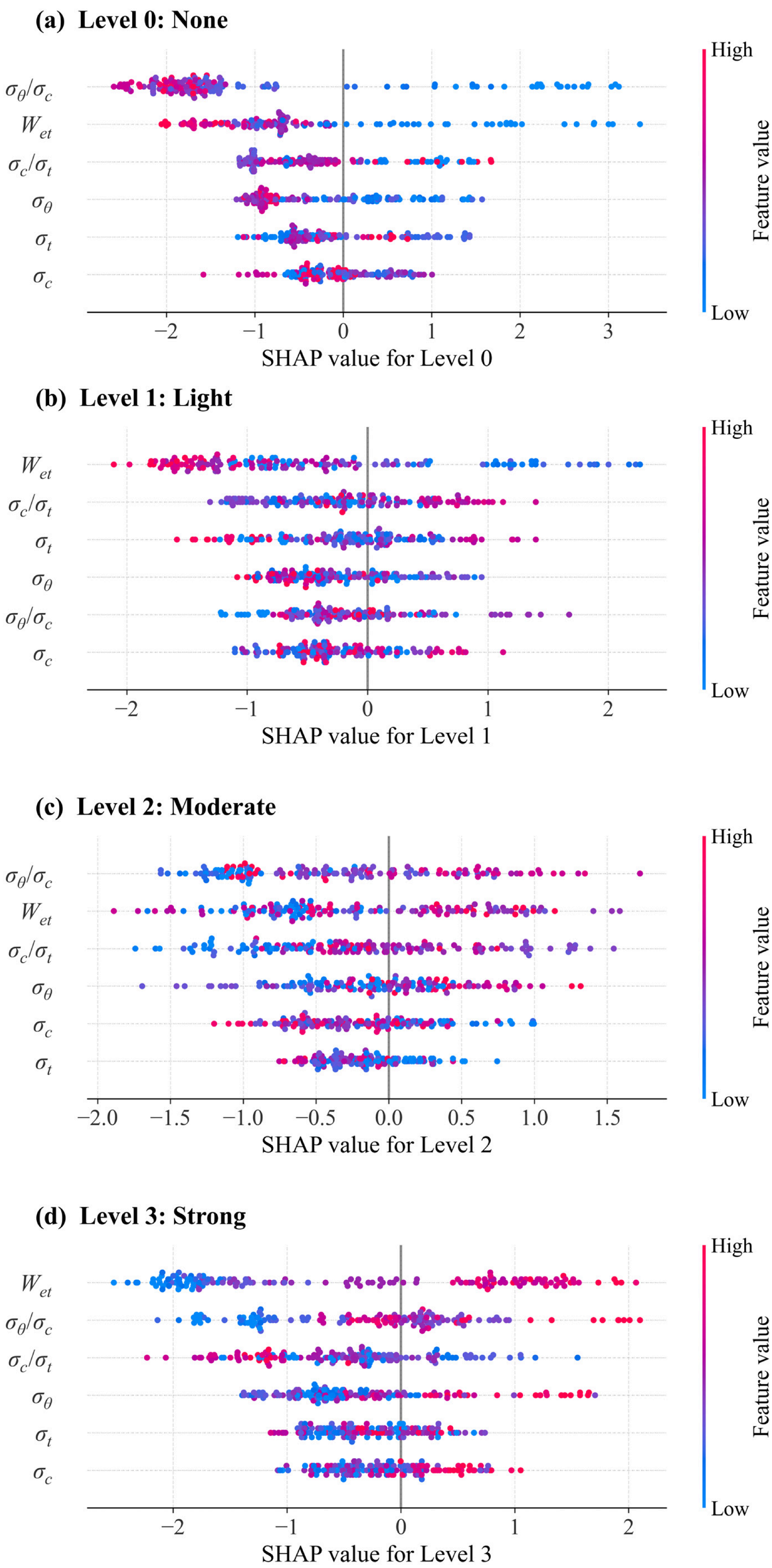

Figure 11. Model interpretability analysis based on BO-XGBoost-SHAP.

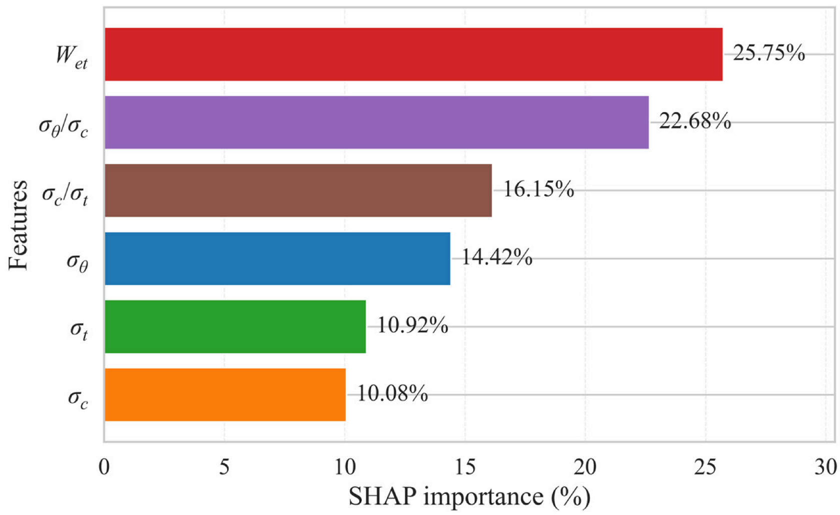

Figure 12. Feature index SHAP importance ranking.

For Level 2 (moderate rockburst), the SHAP distribution range of σ_θ/σ_c, W_{et}, and σ_c/σ_t significantly expands, and the distribution of high eigenvalues in the positive SHAP region increases, indicating that as the rockburst intensity increases, the positive driving effect of stress concentration, energy accumulation, and rock mass brittleness on the model's discrimination results gradually strengthens. In particular, high values of σ_θ/σ_c and W_{et} significantly increase the model's tendency to classify samples as moderate rockburst, indicating that the formation of moderate rockburst is closely related to higher stress levels and elastic energy reserves.

For Level 3 (strong rockburst), the contribution of W_{et} is most prominent. High W_{et} samples are clearly concentrated in the positive SHAP region, while low W_{et} samples are mainly located in the negative SHAP region, indicating that high elastic energy accumulation is the most important criterion for the model to identify strong rockburst. High features of σ_θ/σ_c and σ_θ also largely correspond to positive SHAP values, indicating that high-geostress environments and strong stress concentrations significantly increase the probability of strong rockburst. In contrast, while other values also participate in model decision-making, their SHAP distributions are more dispersed, suggesting that the occurrence of strong rockburst is not solely determined by rock strength parameters, but is jointly controlled by energy reserves, stress state, and rock mass mechanical properties.

In summary, the BO-XGBoost model demonstrates good physical interpretability in determining rockburst levels. Low-level rockburst mainly correspond to low energy accumulation and low stress concentration, while medium- and high-level rockburst exhibit significant high W_{et}, high σ_θ/σ_c, and high σ_θ driving characteristics. The global importance and classification SHAP distribution results together indicate that the elastic energy index, stress concentration, and brittle characteristics are the key controlling factors for rockburst grade identification. These results not only validate the reliability of the BO-XGBoost model in rockburst grade prediction but also further demonstrate that the model can effectively capture the nonlinear coupling relationship between "energy accumulation—stress concentration—brittle failure" during rockburst incubation.

Comparison of SHAP distributions across different rockburst levels reveals that in low-intensity rockburst samples (none rockburst and moderate rockburst), the SHAP values of each feature are generally concentrated near zero, indicating that the model's discrimination of this type of sample relies on the combined effect of multiple features. However, in moderate and strong rockburst samples, the SHAP values of W_{et}, σ_θ, and

σ_θ/σ_c significantly expand positively, indicating that these indices play a dominant role in identifying high-intensity rockbursts.

5.5. Reflections on Safety Management Based on BO-XGBoost-SHAP Analysis Results

From a safety management perspective, the SHAP interpretability analysis of the BO-XGBoost model not only reveals the main influencing factors for rockburst severity assessment but also provides a basis for on-site risk management, early warning classification, and the formulation of prevention and control measures. According to the global importance results of SHAP, the elastic energy index, stress coefficient, and brittleness coefficient are the main factors affecting the model's assessment results, contributing over 60% cumulatively. This indicates that rockburst risk management cannot rely solely on a single strength index but should focus on dynamic control throughout the entire process, considering surrounding rock energy accumulation, stress concentration, and the brittle characteristics of the rock mass.

Firstly, the elastic energy index has the highest importance in the model, indicating that energy accumulation is a key factor in the escalation of rockburst risk. During construction, information such as microseismic monitoring, energy release rate, event frequency, and seismic source concentration can be used to identify areas of rapid energy accumulation or abnormal release. If monitoring results show a continuous increase in the surrounding rock energy level, timely measures should be taken, such as controlling the excavation step distance, reducing blasting disturbance, adjusting the construction pace, and implementing pre-splitting blasting or deep-hole pressure-relief blasting, to prevent the continuous accumulation and sudden release of energy in localized areas. For areas with high rockburst risk, specific construction plans and emergency response plans should be developed in advance to reduce the exposure time of personnel and equipment in high-risk areas.

Secondly, the stress coefficient and the maximum tangential stress also contribute significantly to model decision-making, indicating that high stress concentration is a crucial factor in the occurrence and intensity enhancement of rockburst. Therefore, safety management should strengthen the identification, classification, and tracking control of high stress concentration areas. For high-stress areas, a risk assessment should be conducted before excavation to optimize roadway layout, cross-sectional shape, and excavation sequence, minimizing local stress concentration. During construction, support parameters and stress relief measures should be dynamically adjusted based on monitoring results. For areas with significant stress concentration, abnormal surrounding rock deformation, or increased microseismic activity, proactive control measures such as stress relief holes, stress relief trenches, and stress relief roadways should be implemented promptly, and the frequency of on-site inspections should be increased to prevent rockburst risks from developing from local anomalies into sudden disasters.

Furthermore, although rock strength and brittleness-related indicators rank relatively low in overall importance, they still play a crucial role in determining the boundaries of rockburst severity. For brittle rock formations with low tensile strength, safety management should avoid relying solely on rigid supports. Instead, support systems with energy absorption, pressure relief, and coordinated deformation capabilities should be employed, such as high-prestressed anchor cables, pressure-relief anchors, energy-absorbing components, and combined steel arch and shotcrete support, to improve the impact resistance of the rock-support system. Simultaneously, differentiated support designs should be implemented based on the mechanical properties of the surrounding rock and the rockburst risk level to avoid using the same support standard for different risk areas.

In summary, based on the SHAP analysis results, a rockburst safety management approach can be established, prioritizing energy monitoring, focusing on stress control, and

https://doi.org/10.3390/pr14152450

supplementing with lithology identification. For low-risk areas, routine monitoring and normal support should be the primary methods. For medium-risk areas with high energy accumulation or significant stress concentration, monitoring frequency should be increased and local pressure relief and support reinforcement should be implemented in advance. For high-energy, high-stress, and brittle rockburst risk areas, comprehensive prevention and control measures combining "advanced early warning, active pressure relief, energy-absorbing support, construction control, and emergency preparedness" should be adopted. This management approach can transform model interpretation results into actionable risk control measures on-site, thereby enhancing the engineering application value of rockburst prediction results and providing a scientific basis for safe construction and risk classification management of deep underground engineering.

5.6. Limitations

(1) Limitations in sample source and scale: To alleviate class imbalance, this paper employs the SMOTE method to augment minority class samples. Compared to simple random oversampling methods that directly replicate existing samples, SMOTE generates new synthetic samples in the sample space by analyzing the neighborhood relationships between minority class samples. This improves the diversity of minority class samples and reduces the model's dependence on duplicate samples. However, since the generated samples are based on interpolation relationships between existing minority class samples, some synthetic samples may not fully reflect the physical characteristics of actual rockburst generation processes. Synthetic samples cannot replace real engineering data, and their effectiveness still depends on the representativeness of the original samples.

(2) Limitations in feature indicator selection: The feature parameters selected in this paper mainly focus on stress, rock strength, energy, and brittleness. Although these can reflect the main mechanical characteristics of rockburst occurrence well, they have not fully considered factors such as structural surface development characteristics, construction disturbance methods, and time effects. This, to some extent, limits the model's ability to characterize the multi-scale and multi-process evolution mechanism of rockbursts.

(3) Limitations in model application and engineering verification: While the database in this paper covers a variety of engineering cases, its coverage of engineering types, burial depths, and complex geological environments remains limited due to the availability of existing literature and publicly available engineering data. Therefore, it cannot fully represent all deep underground engineering conditions. Consequently, the model's generalization ability needs further validation using more field monitoring data when facing extreme stress states, special geological conditions, or engineering scenarios not included in the training database.

6. Conclusions

This paper focuses on the prediction and safety management of rockburst disasters in deep underground engineering. Based on multi-source rock mechanics parameters and engineering case data, it systematically conducts research on rockburst level classification and mechanism analysis. By constructing a rockburst sample database containing stress, strength, energy, and brittleness characteristics, various machine learning algorithms are introduced to determine the rockburst level. The model performance and decision-making mechanism are further explored by combining sample balancing, Bayesian optimization, and interpretability analysis methods. Based on this, corresponding rockburst safety management ideas are proposed from an engineering application perspective. The main conclusions are as follows:

(1) The machine learning model constructed based on multi-source rock mechanics parameters can effectively characterize the multi-factor coupling and nonlinear characteristics of rockburst occurrence. By introducing maximum tangential stress, rock strength parameters, elastic energy index, and stress-brittleness comprehensive index, and using the SMOTE method to handle sample imbalance, the established dataset provides a reliable data foundation for rockburst level classification.
(2) In the comparative analysis of six machine learning algorithms, XGBoost models show higher classification accuracy and stability in rockburst level discrimination. Based on the comprehensive accuracy, macro-average F1 score, confusion matrix, and AUC curve results, the integrated tree model has significant advantages in handling the complex nonlinear characteristics of rockburst and multi-level classification problems, and can effectively distinguish rockburst of different intensities.
(3) The SHAP interpretability analysis based on the BO-XGBoost model reveals the intrinsic connection between the model's decision-making mechanism and the physical process of rockburst. Elastic energy index and stress-related indicators play a dominant role in rockburst level prediction, while rock strength and brittleness parameters have a moderating and amplifying effect on rockburst intensity. This result is consistent with the engineering understanding that rockburst are mainly caused by energy accumulation and stress concentration.
(4) Based on the SHAP analysis results, a rockburst safety management approach is proposed, with energy control and stress regulation as the core and rock mechanics properties as a supplement. By implementing graded control, differentiated support, and dynamic monitoring in high-energy and high-stress areas, the scientific nature of rockburst risk identification and prevention can be effectively improved, providing technical support for rockburst safety management and disaster prevention in deep underground engineering.

Author Contributions: Conceptualization, J.Z.; Methodology, J.Z.; Software, J.Z.; Validation, J.Z.; Formal analysis, Z.M.; Investigation, L.J. and Z.M.; Writing—original draft, J.Z. and Z.W.; Writing—review and editing, J.Z. and Z.W.; Supervision, Z.W. All authors have read and agreed to the published version of the manuscript.

Funding: This research received no external funding.

Data Availability Statement: The data presented in this study are openly available in an interpretable rockburst prediction model based on SSA-CatBoost at https://doi.org/10.1016/j.tust.2025.106820, reference number [42].

Conflicts of Interest: Author Zhixin Ma was employed by China Construction Seventh Engineering Bureau Co., Ltd. The remaining authors declare that the research was conducted in the absence of any commercial or financial relationships that could be construed as a potential conflict of interest.

References

1. Lu, J.; Jiang, W.; Xie, H.; Gao, H.; Zhang, D. Dynamic disaster mechanism and acoustic emission evolution of deep coal-rock under true triaxial disturbance stress. *J. Rock Mech. Geotech. Eng.* **2025**, *17*, 5829–5844. [CrossRef]
2. Wang, J.; Dong, L.; Ji, S. Rock mass instability early warning model: A case study of a high and steep annular slope mining areas using Sen's slope trend analysis. *Tunn. Undergr. Space Technol.* **2025**, *159*, 106514. [CrossRef]
3. Wu, M.; Ye, Y.; Wang, Q.; Hu, N. Development of rockburst research: A comprehensive review. *Appl. Sci.* **2022**, *12*, 974. [CrossRef]
4. Waqar, M.F.; Guo, S.; Qi, S. A comprehensive review of mechanisms, predictive techniques, and control strategies of rockburst. *Appl. Sci.* **2023**, *13*, 3950. [CrossRef]

5. Dong, L.; Huang, X.; Li, S.; Wang, J. Research on microseismic parameter prediction for rock mass instability disasters based on time series models. *J. Appl. Geophys.* **2026**, *250*, 106278. [CrossRef]
6. Hosseini, S.; Armaghani, D.J.; He, X.; Pradhan, B.; Zhou, J.; Sheng, D. Fuzzy cognitive map for evaluating critical factors causing rockbursts in underground construction: A fundamental study. *Rock Mech. Rock Eng.* **2024**, *57*, 9713–9738. [CrossRef]
7. Waqar, M.F.; Qi, S.; Zheng, B.; Guo, S. Dynamic testing methods and failure properties of rocks: A comprehensive review. *Rock Mech. Rock Eng.* **2025**, 1–51. [CrossRef]
8. Zhang, Q.; Li, W.; Yuan, L.; Zheng, T.; Liang, Z.; Wang, X. A review of tunnel rockburst prediction methods based on static and dynamic indicators. *Nat. Hazards* **2024**, *120*, 10465–10512. [CrossRef]
9. Khan, M.; He, X.; Guo, J.; Song, D. Accurate prediction of indicators for engineering failures in complex mining environments. *Eng. Fail. Anal.* **2024**, *155*, 107736. [CrossRef]
10. Cortés, N.; Hekmatnejad, A.; Pan, P.; Mohtarami, E.; Pena, A.; Taheri, A.; González, C. Empirical approaches for rock burst prediction: A comprehensive review and application to the new level of El Teniente Mine, Chile. *Heliyon* **2024**, *10*, e26515. [CrossRef] [PubMed]
11. Owusu-Ansah, D.; Tinoco, J.; Lohrasb, F.; Martins, F.; Matos, J. A decision tree for rockburst conditions prediction. *Appl. Sci.* **2023**, *13*, 6655. [CrossRef]
12. Sun, J.; Wang, W.; Xie, L. Predicting short-term rockburst using RF–CRITIC and improved cloud model. *Nat. Resour. Res.* **2024**, *33*, 471–494.
13. Hafiz, H.; Li, D.; Luo, P.; Rasa, A.R.; Yang, B. Interpretable k-nearest neighbors for rockburst risk prediction: Robust performance and mechanistic insights for deep rock engineering. *Eng. Fail. Anal.* **2025**, *186*, 110443. [CrossRef]
14. Hu, X.; Huang, L.; Chen, J.; Li, X.; Zhang, H. Rockburst prediction based on optimization of unascertained measure theory with normal cloud. *Complex Intell. Syst.* **2023**, *9*, 7321–7336. [CrossRef]
15. Chuai, X.; Shu, L.; Huo, Z.; Liu, Z. Analytical Hierarchy Process–Fuzzy Comprehensive Evaluation Model for Predicting Rockburst with Multiple Indexes. *Appl. Sci.* **2025**, *15*, 11708. [CrossRef]
16. Xue, Y.; Bai, C.; Kong, F.; Qiu, D.; Li, L.; Su, M.; Zhao, Y. A two-step comprehensive evaluation model for rockburst prediction based on multiple empirical criteria. *Eng. Geol.* **2020**, *268*, 105515. [CrossRef]
17. Kim, H.; Kim, J. Long-term prediction of safety parameters with uncertainty estimation in emergency situations at nuclear power plants. *Nucl. Eng. Technol.* **2023**, *55*, 1630–1643. [CrossRef]
18. Qiu, Y.; Zhou, J. Short-term rockburst damage assessment in burst-prone mines: An explainable XGBOOST hybrid model with SCSO algorithm. *Rock Mech. Rock Eng.* **2023**, *56*, 8745–8770. [CrossRef]
19. Ma, T.H.; Tang, C.A.; Tang, S.B.; Kuang, L.; Yu, Q.; Kong, D.-Q.; Zhu, X. Rockburst mechanism and prediction based on microseismic monitoring. *Int. J. Rock Mech. Min. Sci.* **2018**, *110*, 177–188. [CrossRef]
20. Li, X.; Chen, D.; Fu, J.; Liu, S.; Geng, X. Construction and application of fuzzy comprehensive evaluation model for rockburst based on microseismic monitoring. *Appl. Sci.* **2023**, *13*, 12013. [CrossRef]
21. Di, Y.; Wang, E.; Huang, T. Identification method for microseismic, acoustic emission and electromagnetic radiation interference signals of rock burst based on deep neural networks. *Int. J. Rock Mech. Min. Sci.* **2023**, *170*, 105541. [CrossRef]
22. Yang, H.; Wang, E.; Song, Y.; Chen, D.; Wang, X.; Wang, D.; Li, J. Identification and prediction method for acoustic emission and electromagnetic radiation signals of rock burst based on deep learning. *Phys. Fluids* **2024**, *36*, 076624. [CrossRef]
23. Wang, D.; Ma, Y.; Liu, X.; Li, D.; Liu, Q.; Yang, H.; Li, X. Improving mining sustainability and safety by monitoring precursors of Catastrophic failures in loaded granite: An experimental study of Acoustic Emission and Electromagnetic Radiation. *Sustainability* **2024**, *16*, 1045. [CrossRef]
24. Zhao, S.; Wang, E.; Wang, J.; Jia, H.; Zhang, Q.; Li, Z. Multi-level Fusion Early Warning of Rock Burst Utilizing Acoustic Emission and Electromagnetic Radiation Chaotic Prediction and Image Feature Mining: Case Studies. *Rock Mech. Rock Eng.* **2025**, *58*, 14021–14044. [CrossRef]
25. Li, X.; Zhou, J.; Yang, Z.; Li, H.; Bu, J.; Liu, Z.; Wang, Y. Time-frequency evolution of electromagnetic radiation in deformation and fracture of composite coal-rock under different loading rates. *Constr. Build. Mater.* **2024**, *453*, 139030. [CrossRef]
26. Zhu, B.; Fan, J.; Shi, X.; Liu, P.; Guo, J. Study on rockburst proneness of deep tunnel under different geo-stress conditions based on DEM. *Geotech. Geol. Eng.* **2022**, *40*, 1373–1386.
27. Zhang, L.; Zhang, X.; Wu, J.; Zhao, D.; Fu, H. Rockburst prediction model based on comprehensive weight and extension methods and its engineering application. *Bull. Eng. Geol. Environ.* **2020**, *79*, 4891–4903. [CrossRef]
28. Faradonbeh, R.S.; Taheri, A.; Karakus, M. The propensity of the over-stressed rock masses to different failure mechanisms based on a hybrid probabilistic approach. *Tunn. Undergr. Space Technol.* **2022**, *119*, 104214. [CrossRef]
29. Papadopoulos, D.; Benardos, A. Combining machine learning and numerical modelling for rockburst prediction. *Geomech. Geoengin.* **2024**, *19*, 183–198.
30. Ma, C.; Yuan, Y.; Ji, X.; Peng, F.; Chen, Z.; Zhang, H. Analysis of key geological structures and rockburst prediction method. *Sci. Rep.* **2025**, *15*, 16031. [CrossRef] [PubMed]

31. Liu, X.; Zhu, W.; Han, Y.; Guan, K.; Qin, R. Experiments and numerical simulations of rockburst prevention based on the slotting method. *Bull. Eng. Geol. Environ.* **2023**, *82*, 383. [CrossRef]
32. Zhang, R.; Liu, Y.; Hou, S. Evaluation of rockburst risk in deep tunnels considering structural planes based on energy dissipation rate criterion and numerical simulation. *Tunn. Undergr. Space Technol.* **2023**, *137*, 105128. [CrossRef]
33. Wang, J.; Ma, H.; Yan, X. Rockburst intensity classification prediction based on multi-model ensemble learning algorithms. *Mathematics* **2023**, *11*, 838. [CrossRef]
34. Wang, J.; Dong, L. Risk assessment of rockburst using SMOTE oversampling and integration algorithms under GBDT framework. *J. Cent. South Univ.* **2024**, *31*, 2891–2915. [CrossRef]
35. Waqar, M.F.; Qi, S.; Guo, S.; Wang, Z.; Zheng, B.; Pervaiz, M. Machine Learning-Based Permeability Prediction for CO_2 Storage: A Case Study from the Petrel Sub-basin, Australia. *Geomech. Energy Environ.* **2026**, *47*, 100867. [CrossRef]
36. Li, N.; Feng, X.; Jimenez, R. Predicting rock burst hazard with incomplete data using Bayesian networks. *Tunn. Undergr. Space Technol.* **2017**, *61*, 61–70. [CrossRef]
37. Li, T.; Li, Y.; Yang, X. Rock burst prediction based on genetic algorithms and extreme learning machine. *J. Cent. South Univ.* **2017**, *24*, 2105–2113. [CrossRef]
38. Lin, Y.; Zhou, K.; Li, J. Application of cloud model in rock burst prediction and performance comparison with three machine learning algorithms. *IEEE Access* **2018**, *6*, 30958–30968. [CrossRef]
39. Shirani Faradonbeh, R.; Taheri, A. Long-term prediction of rockburst hazard in deep underground openings using three robust data mining techniques. *Eng. Comput.* **2019**, *35*, 659–675.
40. Pu, Y.; Apel, D.B.; Lingga, B. Rockburst prediction in kimberlite using decision tree with incomplete data. *J. Sustain. Min.* **2018**, *17*, 158–165. [CrossRef]
41. Ghasemi, E.; Gholizadeh, H.; Adoko, A.C. Evaluation of rockburst occurrence and intensity in underground structures using decision tree approach. *Eng. Comput.* **2020**, *36*, 213–225.
42. Xue, Y.; Bai, C.; Qiu, D.; Kong, F.; Li, Z. Predicting rockburst with database using particle swarm optimization and extreme learning machine. *Tunn. Undergr. Space Technol.* **2020**, *98*, 103287. [CrossRef]
43. Shukla, R.; Khandelwal, M.; Kankar, P.K. Prediction and assessment of rock burst using various meta-heuristic approaches. *Min. Metall. Explor.* **2021**, *38*, 1375–1381. [CrossRef]
44. Bao, G.; Hou, K.; Sun, H. Rock Burst intensity-grade prediction based on comprehensive weighting method and bayesian optimization algorithm–improved-support vector machine model. *Sustainability* **2023**, *15*, 15880. [CrossRef]
45. Yan, S.; Liu, R.; Zhang, Y.; Yao, X.; Yang, Y.; Wang, Q.; Guo, B.; Wang, S. Investigation and application of data balancing and combined discriminant model in rock burst severity prediction. *Sci. Rep.* **2024**, *14*, 29657. [CrossRef] [PubMed]
46. Keller, J.M.; Gray, M.R.; Givens, J.A. A fuzzy k-nearest neighbor algorithm. *IEEE Trans. Syst. Man Cybern.* **1985**, *15*, 580–585. [CrossRef]
47. Suthaharan, S. Support vector machine. In *Machine Learning Models and Algorithms for Big Data Classification: Thinking with Examples for Effective Learning*; Springer: Boston, MA, USA, 2016; pp. 207–235.
48. Myles, A.J.; Feudale, R.N.; Liu, Y.; Woody, N.A.; Brown, S.D. An introduction to decision tree modeling. *J. Chemom.* **2004**, *18*, 275–285. [CrossRef]
49. Biau, G.; Scornet, E. A random forest guided tour. *Test* **2016**, *25*, 197–227. [CrossRef]
50. Popescu, M.C.; Balas, V.E.; Perescu-Popescu, L.; Mastorakis, N. Multilayer perceptron and neural networks. *WSEAS Trans. Circuits Syst.* **2009**, *8*, 579–588.
51. Chen, T. XGBoost: A Scalable Tree Boosting System. In *Proceedings of the 22nd ACM SIGKDD International Conference on Knowledge Discovery and Data Mining*; Cornell University: Ithaca, NY, USA, 2016.
52. Sokolova, M.; Lapalme, G. A systematic analysis of performance measures for classification tasks. *Inf. Process. Manag.* **2009**, *45*, 427–437. [CrossRef]
53. Kong, W.; Hou, P.; Liang, X.; Gao, F.; Liu, Q. An interpretable rockburst prediction model based on SSA-CatBoost. *Tunn. Undergr. Space Technol.* **2025**, *164*, 106820. [CrossRef]
54. Chawla, N.V.; Bowyer, K.W.; Hall, L.O.; Kegelmeyer, W.P. SMOTE: Synthetic minority over-sampling technique. *J. Artif. Intell. Res.* **2002**, *16*, 321–357. [CrossRef]